Bioactive DNA-Peptide Nanotubes Enhance the Differentiation of Neural Stem Cells Into Neurons

Nicholas Stephanopoulos[1], Ronit Freeman[1], Hilary A. North[2], Shantanu Sur[1], Su Ji Jeong[2], Faifan Tantakitti[1,3], John A. Kessler[2], Samuel I. Stupp[1,3,4,5]

1. Simpson Querrey Institute for BioNanotechnology, Feinberg School of Medicine, Northwestern University, Chicago, IL 60611, USA
2. Department of Neurology, Northwestern University, Chicago, IL 60611, USA
3. Department of Materials Science and Engineering, Northwestern University, Evanston, IL 60208, USA
4. Department of Chemistry, Northwestern University, Evanston, IL 60208, USA
5. Department of Medicine, Northwestern University, Chicago, IL 60611, USA

Supporting Information

Materials: All chemicals were purchased from commercial vendors and used without further purification. Dibenzocyclooctyne-sulfo-N-hydroxysuccinimidyl ester (DIBAC-sulfo-NHS) was purchased from Sigma-Aldrich, dissolved in DMSO to a concentration of 100 mM, and stored at -20 °C. All DNA strands were purchased without additional purification from Integrated DNA Technologies (IDT), dissolved at 1 mM in water, and stored at -20 °C prior to use. APTES-coated glass coverslips were purchased from SCHOTT.

Peptide synthesis: The F^{az}GGRGDS and F^{az}GGRGES peptides (Figure S1) were synthesized at the Peptide Synthesis Core at the Simpson Querrey Institute for BioNanotechnology using standard fluoren-9-ylmethoxycarbonyl (Fmoc) solid-phase peptide synthesis on rink amide MBHA resin (100-200 mesh, 0.55 mmol/gram). fluoren-9-ylmethoxycarbonyl (Fmoc) solid-phase peptide synthesis on rink amide MBHA resin (100-200 mesh, 0.55 mmol/gram). Following synthesis, each peptide was cleaved from the resin in a mixture of 95% trifluoroacetic acid (TFA), 2.5 % triisopropyl silane (TIS), 2.5% water. The solvent was removed under reduced pressure and the peptide was precipitated using cold diethyl ether. The precipitate was filtered and washed with ether, then dissolved in water with 0.1% TFA. The solution was purified using reverse phase HPLC (Varian Prostar 363, Jupiter 10u Proteo 90A column) using a water/acetonitrile gradient (2-50% acetonitrile over 30 minutes) with 0.1% TFA. Purified peptides were lyophilized, and stored at -20 °C. The purity of the peptides was confirmed by electrospray ionization mass spectrometry in positive mode (ESI-MS, Agilent 6510 Q-TOF).

DNA-peptide conjugation: To a solution of s1a-3'amine DNA (1 mM in H_2O) was added 1/5 volume of 100 mM phosphate buffer (pH 8.5). To this solution was added dibenzocyclooctyne-sulfo-N-hydroxysuccinimidyl ester (as a 100 mM solution in DMSO) to a final concentration of 10 mM (~10 eq., 10% total DMSO), and the mixture was reacted for 2 h at RT, with vigorous shaking. Excess small molecule was removed using a size exclusion spin column (Illustra Microspin G-25, GE Healthcare) pre-equilibrated with 20 mM phosphate, pH 7.5 buffer. To this solution was added

two volumes of the azido-peptide (either F^{az}GGRGDS or F^{az}GGRGES) as a 1 mM solution in water, for a final concentration of 333 μM DNA and 667 μM peptide (2 eq.). Sodium chloride was added to a final concentration of 100 mM and the reaction mixture was gently agitated overnight. Following reaction, excess peptide was removed by spin-concentration three times (Amicon Ultra spin concentrators, 3,000 Da molecular weight cutoff, Millipore) using 50 mM triethylammonium acetate (TEAA) buffer, pH 7, prior to purification by reverse phase HPLC.

DNA-peptide purification: The DNA-peptide conjugates were purified using reverse phase HPLC (Agilent 1260 Infinity, DIKMA Inspire C18 column (5 um, 250 x 4.6 mm)) using a gradient of organic buffer B (90% acetonitrile in water, + 50 mM TEAA, pH 7) in water + 50 mM TEAA, pH 7 (buffer A). The TEAA buffer is critical for desalting the DNA (through the use of a spin concentrator, as described above) and for its retention on the C18 column. Separation was achieved using a gradient of 0-40% buffer B over 30 minutes, and DNA was detected by monitoring absorbance at 260 nm. As shown in Figure S2a, unmodified s1a-3'amine eluted at 10-11 min, whereas the s1a-3'RGDS conjugate eluted at 17-18 min. The s1a-3'RGES conjugate had an identical trace to the RGDS conjugate. While it was possible to isolate the DNA-cyclooctyne conjugate by reverse phase HPLC prior to reaction with the azido-peptides, we found that no intermediate purification was necessary, and the unmodified s1a-3'amine DNA did not interfere with the click reaction. The purity of the DNA-peptide conjugates was confirmed by electrospray ionization mass spectrometry in negative mode (ESI-MS, Agilent 6510 Q-TOF).

Nanotube annealing: To form the DNA nanotubes, equal amounts of all constituent strands (25 μM) were mixed in TAE/Mg buffer, pH 8.3 (40 mM Tris, 20 mM acetic acid, 1 mM EDTA, 12.5 mM $Mg(OAc)_2$). The mixture was annealed from 95 °C to 25 °C over 5 h. After annealing, the solutions were stored at 4 °C prior to coating the APTES slides. All DNA samples were used within 12 h of annealing to coat slides.

Conventional TEM imaging: Following annealing, DNA nanotube solutions were applied to copper mesh TEM grids (Electron Microscopy Science) for 5 min. Following wicking and rinsing with water, the grids were stained with 2% uranyl acetate solution (twice for 30 s) and dried for 15 min prior to imaging. Grids were imaged with a FEI Spirit G2 TEM.

Cryogenic TEM imaging: Cryo-TEM images were acquired on a JEOL 1230 microscope operating at an accelerating voltage of 100 kV. Samples were prepared on a 300 mesh copper grid with either a lacey carbon support or QUANTIFOIL®–Holey carbon support (Electron Microscopy Sciences). The grids were first treated with air plasma (Harrick Plasma) for 30 s prior to use. Then, the solution (6.5ul, 25 μM total DNA concentration after annealing, in TAE/Mg buffer) was deposited on a grid, blotted using a Vitrobot Mark IV (FEI) vitrification robot at 90-100% humidity, and vitrified by plunging the grid into a liquid ethane reservoir. The samples were placed into a Gatan 626 cryo-holder under liquid nitrogen, and a Gatan 831 bottom-mounted CCD camera was used to acquire the image.

Surface coating: Nanotube solutions following annealing (25 μM total DNA concentration) were drop-cast on APTES-modified slides and incubated at 37 °C overnight to allow adhesion on the surface. Following incubation, the solution was removed and the slides were rinsed twice with

sterile PBS prior to cell plating.

Fluorescence imaging: Fluorescent DNA nanotubes and controls were prepared by incorporating a 3' fluorescein dye in the strand s3. Following annealing, the DNA solutions were coated on APTES-modified slides by drop-casting as described in the surface coating section. Images of the coatings were obtained using an inverted confocal laser scanning microscope (Nikon A1R) working under 60X oil immersion objective. A Z-series stack was acquired to estimate the approximate thickness of the coating.

Fibroblast adhesion experiments: NIH-3T3 murine embryonic fibroblasts were maintained in Dulbecco's modified Eagle's medium (DMEM) with high glucose supplemented with 10% fetal bovine serum (FBS) and 1% penicillin/streptomycin (P/S) and passaged every 3 days. Cells were plated on APTES coverslips coated with either **bare-NT**, **RGDS-NT**, or no coating and left to adhere and spread for 3 h at 37 °C and 5% CO_2. Following adhesion, the culture medium was removed and cells were fixed by exposure for 15 min to 4% paraformaldehyde in PBS. The cells were washed three times with PBS and incubated for 5 min with 0.4% Triton-X to permeabilize the cell membrane. The cells were washed three times with PBS and stained with AlexaFluor-488 conjugated phalloidin to stain the actin filaments and 4',6-diamidino-2-phenylindole (DAPI) to stain the nuclei.

After staining the cells, the coverslips were mounted and imaged using a TissueGnostics cell imaging and analysis system mounted to an upright microscope (TissueFaxs). Morphological quantification of the cells was performed on phalloidin-stained images obtained at 20x objective magnification (TissueGnostics). Acquired images were thresholded using ImageJ software (NIH) and analyzed using routines written in ImageJ software. Projected cell surface area was defined by the phalloidin positive pixels occupied by a cell. For accurate comparison, quantification was performed on at least 250 randomly selected cells from two independent coverslips. Cell morphology data sets were tested for statistical significance using a one-way ANOVA with Bonferroni correction.

Neural stem cell (NSC) experiments: NSCs were isolated from postnatal day 1 mouse subventricular zone and grown as neurospheres in suspension in EGF-containing NSC media with passages every 4 days until three passages had been completed. Upon the third passage, dissociated cells were plated on top of either bare or DNA-coated coverslips at a density of 50,000 cells/ml in very low EGF concentration (0.5 ng/mL) and allowed to differentiate for 7 days. Coverslips were harvested by fixation in 4% paraformaldehyde and immunocytochemistry to identify neurons (with anti-MAP2), astrocytes (with anti-GFAP), and progenitor cells (with anti-Nestin) was performed. Cells were scored as an astrocyte or neuron based on expression of GFAP or MAP2, respectively, and taken as a percentage of the DAPI in each field. Areas of overlapping cells in aggregates were disregarded in order to avoid the confounding effect of cell-cell contact on differentiation. At least 500 cells were counted for each condition in each independent experiment. p values were calculated based on ANOVA.

DNA sequences: The DNA sequences used for construction of the systems described were adapted from Ref. 31. Sequences with a 3' amine for peptide conjugation had a 5T spacer appended at

the 3’ end, followed by IDT’s C6 spacer and the amine modification.

s1: 5’ – CTC AGT GGA CAG CCG TTC TGG AGC GTT GGA CGA AAC T – 3’
s2: 5’ – GTC TGG TAG AGC ACC ACT GAG AGG TA – 3’
s3: 5’ – CCA GAA CGG CTG TGG CTA AAC AGT AAC CGA AGC ACC AAC GCT – 3’
s4: 5’ – CAG ACA GTT TCG TGG TCA TCG TAC CT – 3’
s5: 5’ – CGA TGA CCT GCT TCG GTT ACT GTT TAG CCT GCT CTA C – 3’
s1a: 5’ – CTC AGT GGA CAG CC TTTTT-[C6-amine] – 3’
s1b: 5’ – G TTC TGG AGC GTT GGA CGA AAC T – 3’

For generating fluorescent tubes, the s3 sequence was ordered from IDT with a 3’-fluorescein (FAM) modification.

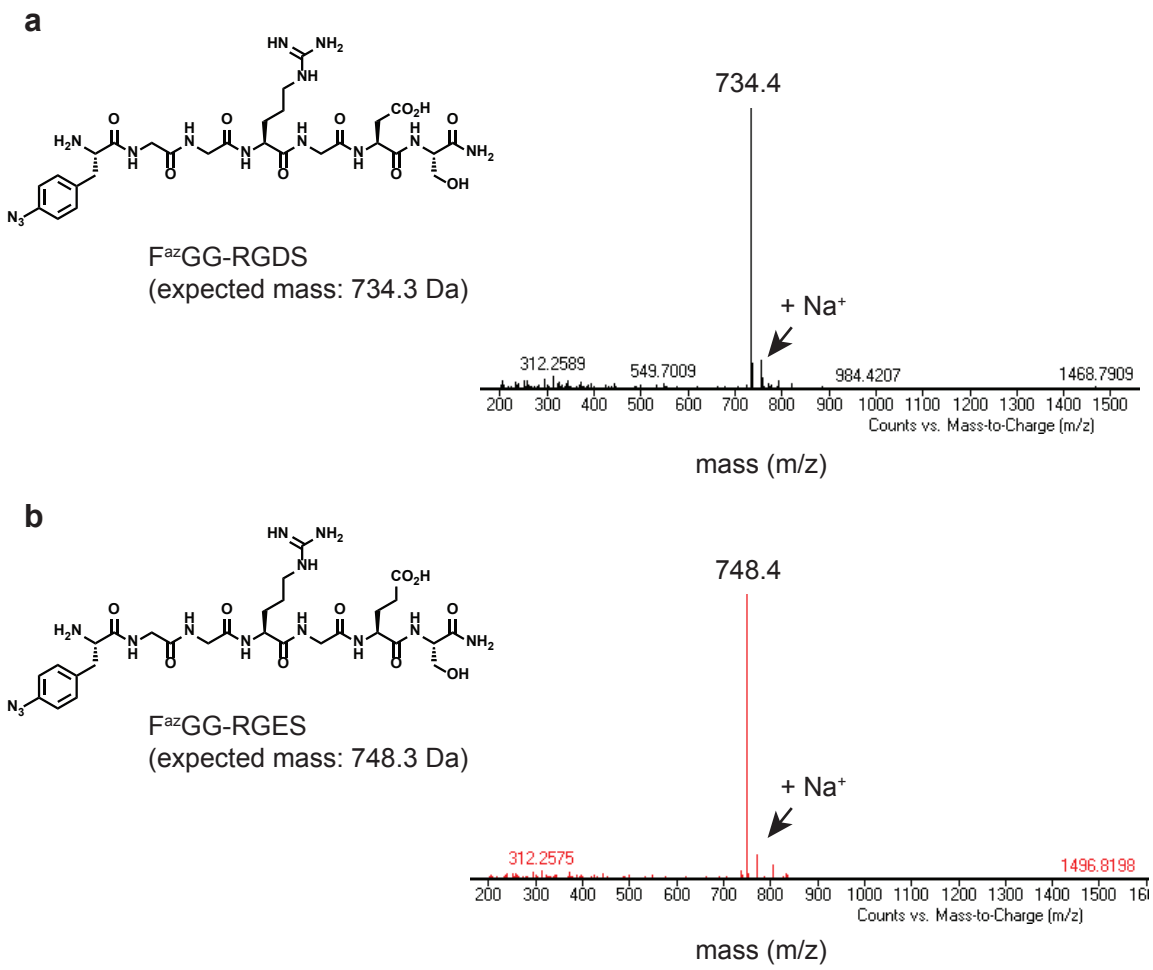

Figure S1: Electrospray ionization mass spectrometry (ESI-MS) analysis of peptides. The peptides F^{az}GGRGDS (a) and F^{az}GGRGES (b) were synthesized by solid-phase peptide synthesis and purified by reverse phase HPLC. ESI-MS analysis confirmed that their identity and high purity.

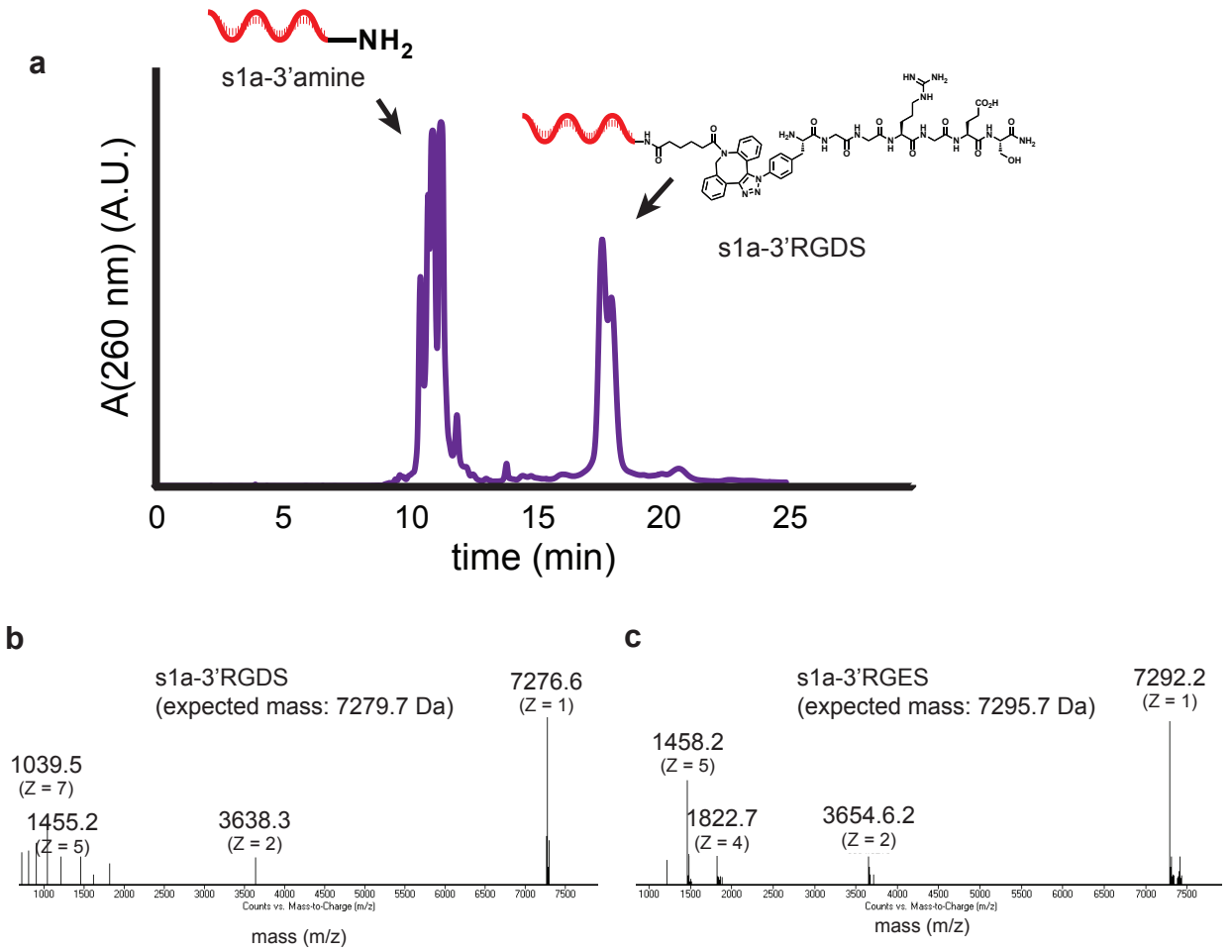

Figure S2: Purification and characterization of DNA-peptide conjugates. (a) Reverse phase HPLC purification (monitoring DNA absorbance at 260 nm) of the s1a-3'RGDS conjugate. Unreacted s1a-3'amine elutes at 10-12 min, whereas the DNA-peptide conjugate elutes at 22-23 min. The trace shown is for the s1a-3'RGDS conjugate; the chromatograph of the s1a-3'RGES conjugate is identical. The identity of the DNA-peptide constructs was verified using ESI-MS. Both the s1a-3'RGDS (b) and s1a-3'RGES (c) conjugates were isolated as highly pure materials, with no unmodified DNA or free peptide.

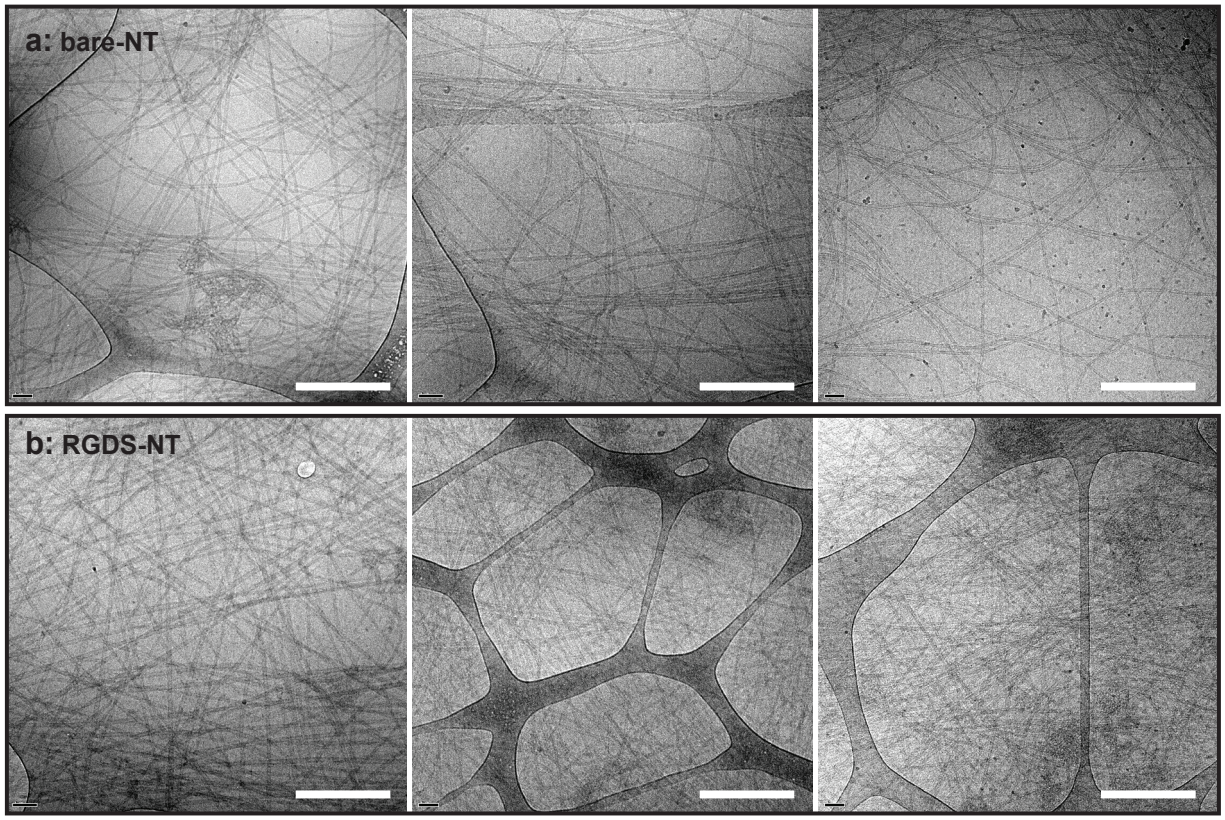

Figure S3: Additional cryo-TEM images of bare-NT and RGDS-NT. Cryogenic transmission electron microscopy images of the **bare-NT** (a) and **RGDS-NT** (b) systems to show the tube structures obtained. Scale bars: 500 nm.

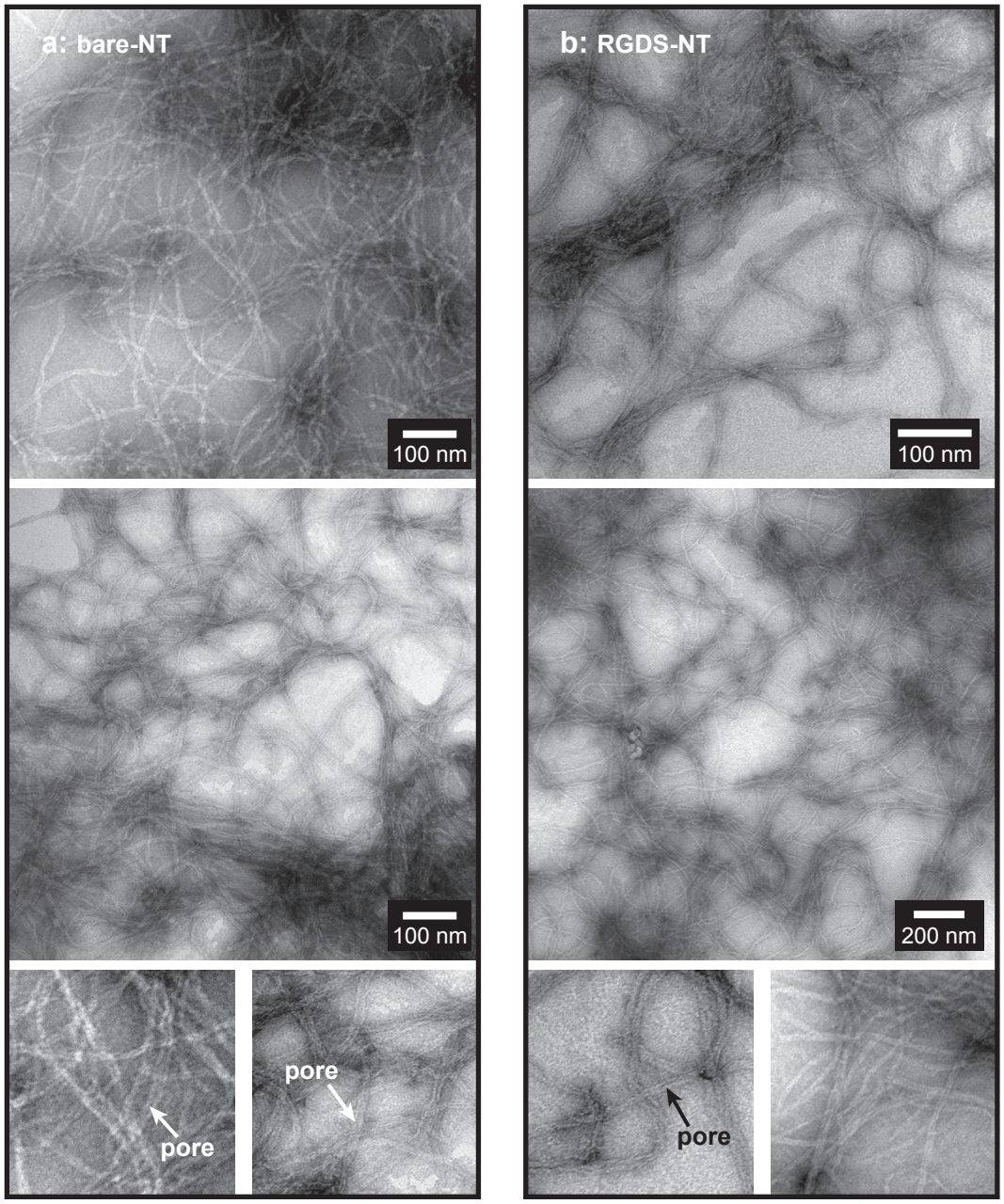

Figure S4: Transmission electron microscopy (TEM) analysis of DNA nanotubes. Conventional TEM analysis (following staining with uranyl acetate) of the **bare-NT** (a) and **RGDS-NT** (b) systems. The long tube-like morphology can be clearly seen (including the pore down the center). There is no observable difference between the unmodified and RGDS-modified tubes.

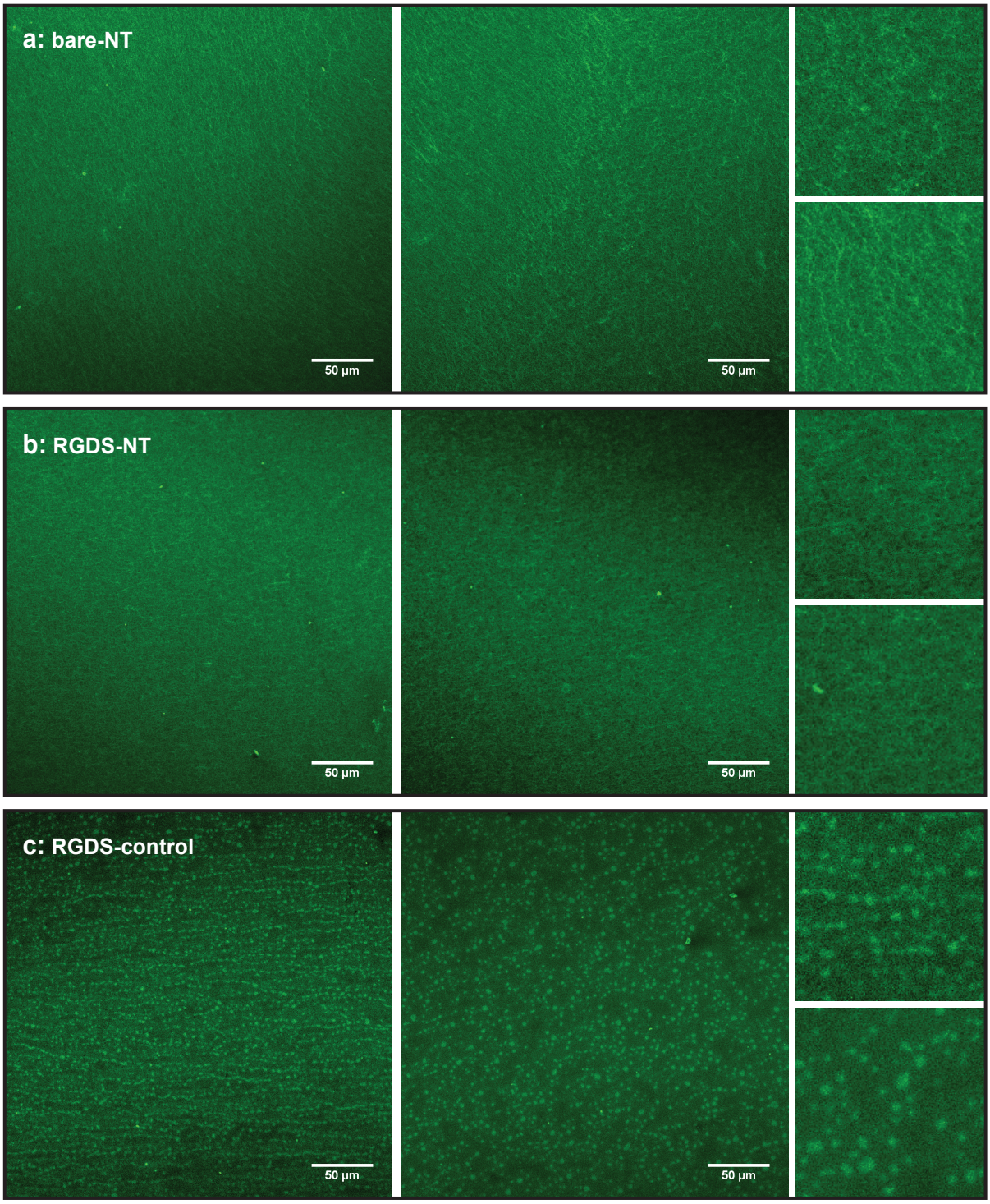

Figure S5: Additional fluorescence images of DNA-modified surfaces. Additional and larger images of the **bare-NT** (a), **RGDS-NT** (b), and **RGDS-control** (c) systems to highlight the differences between them. Insets show magnified areas from the different samples. Both **bare-NT** and **RGDS-NT** show dense mats of fluorescent fiber-like material, whereas **RGDS-control** shows spherical/globular aggregates.

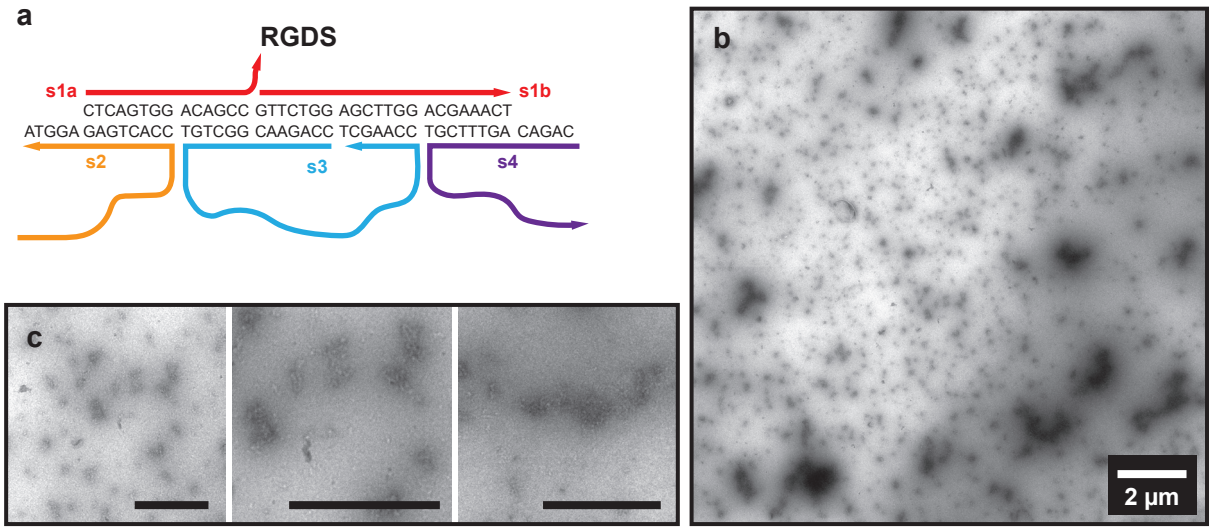

Figure S6: Characterization of the RGDS-control system. (a) Schematic illustration of the tile used. Omitting strand s5 prevents assembly of the "lower" helix and does not allow formation of a tile or nanotube. Nucleotide letters are only shown for the double-stranded portions. (b) Conventional TEM analysis shows a large number of undefined aggregates, but no nanotube structures. (c) Zoomed in TEM images of the aggregates. Scale bars in c: 1 µm.

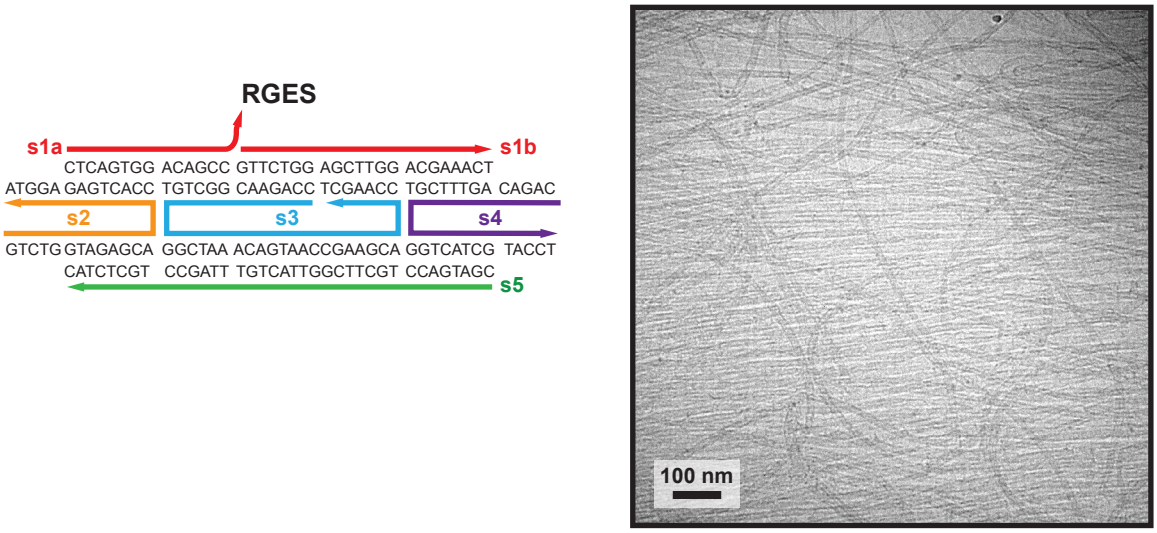

Figure S7: Cryo-TEM analysis of RGES-NT. Including s1a-3'RGES strand resulted in tubes (the "**RGES-NT**" system) that were indistinguishable from the **RGDS-NT** and **bare-NT** systems.

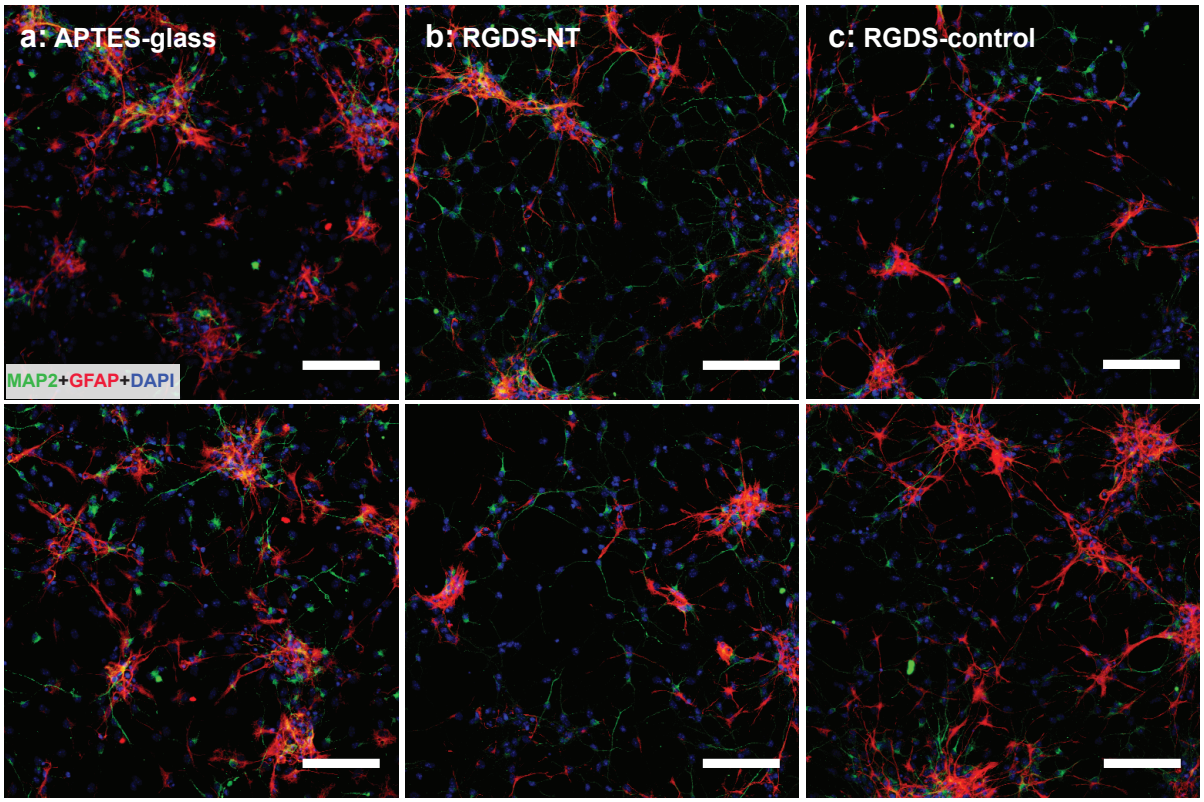

Figure S8: Additional images of NSC differentiation. Additional representative images of the three samples quantified in Fig. 5E, demonstrating cell adhesion, the relative number of neurons and astrocytes, and the morphology of the cells. Scale bars: 100 μm.

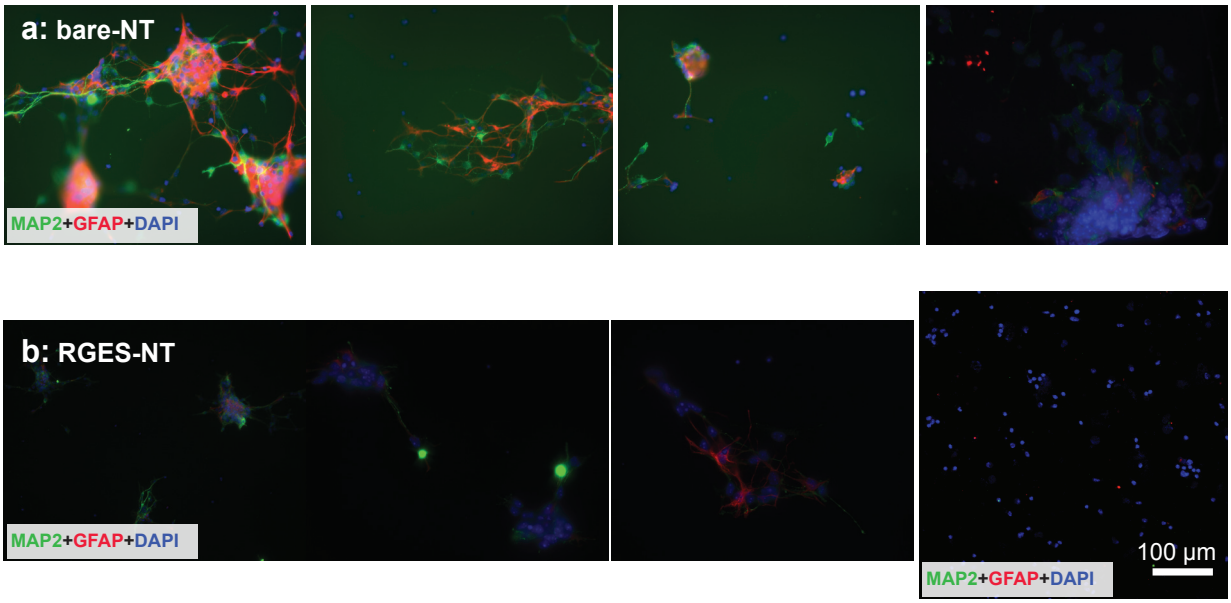

Figure S9: Additional images of poor cell-adhesive substrates. (a) The **bare-NT** sample shows poor cell adhesion (with sparse cell density) and widespread clumping, which makes cell fate highly dependent on cell-cell contact. (b) The **RGES-NT** coatings, which have an epitope that does not bind to integrin receptors, show similar cell-cell aggregation to the **bare-NT** sample in many areas. In some areas, the cells are well distributed (see last image in (b)), but do not stain for either MAP2 or GFAP, indicating a failure to differentiate into any of the lineages as the cells on the other surfaces. The nuclear morphology (from the DAPI stain) indicates that the cells are healthy and alive, but do not express the neuronal or glial markers tested.

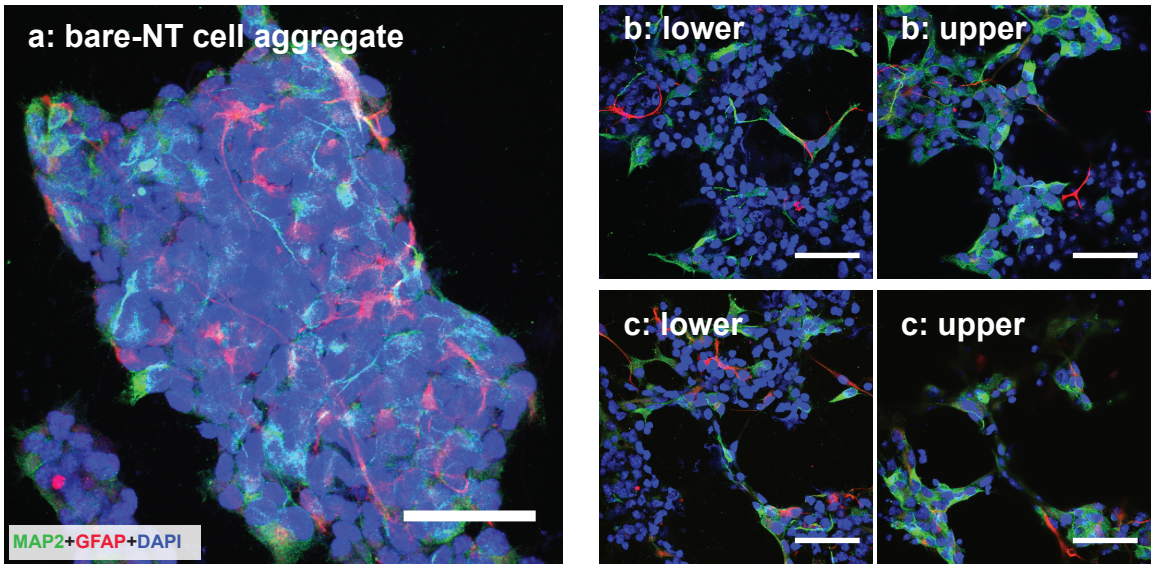

Figure S10: Confocal microscopy imaging of NSC aggregates. (a) Example of extensive aggregation in the **bare-NT** sample, demonstrating that virtually all the NSCs are contacting one another, so it is not possible to control for the influence of cell-cell contact on differentiation. Similar aggregates were seen in the **RGES-NT** sample. (b,c) Confocal microscope slices at different z values to demonstrate that in many of the aggregates cells were on top of other cells, and thus not contacting the DNA substrate. The “lower” images show cells touching the surface. Scale bars: 50 μm.

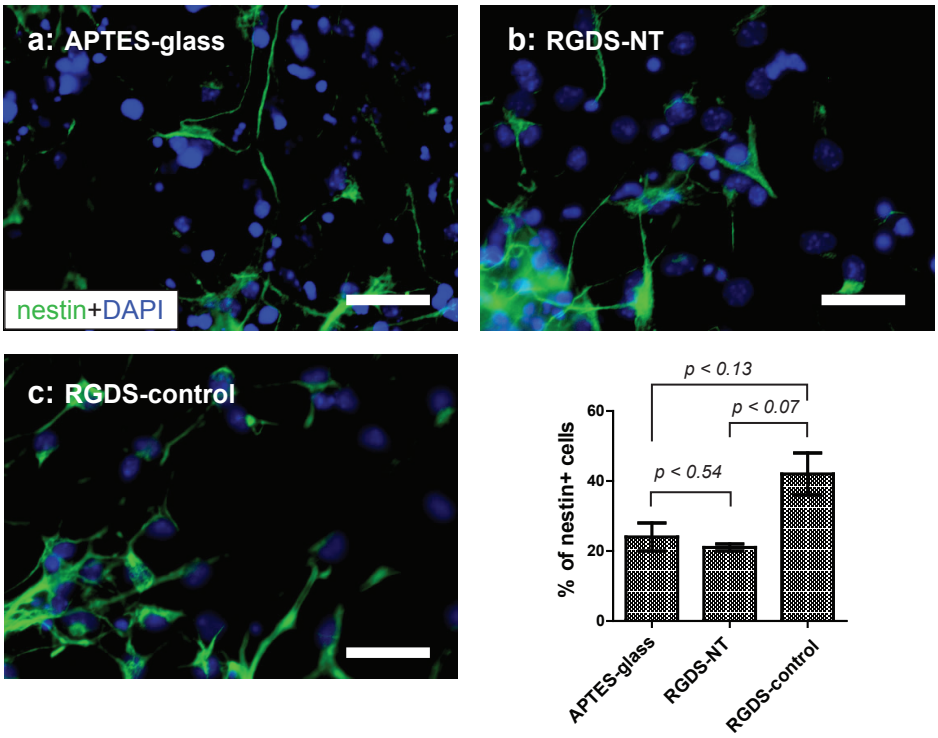

Figure S11: Nestin staining results. NPCs were stained for nestin expression, which indicates an undifferentiated, stem-like state. The **RGDS-ctrl** system showed a trend towards increased nestin expression compared to both the **APTES-glass** and **RGDS-NT** systems. (n = 2; p values calculated using Student's t-test). Scale bars: 20 μm.